Diagnosing CO_2 fluxes in the upwelling system off the Oregon-California coast

Zhimian Cao[1†], Minhan Dai[1]*, Wiley Evans[2,3], Jianping Gan[4], Richard Feely[2]

[1]State Key Laboratory of Marine Environmental Science, Xiamen University, Xiamen, China

[2]Pacific Marine Environmental Laboratory, National Oceanic and Atmospheric Administration, Seattle, Washington, USA

[3]Ocean Acidification Research Center, School of Fisheries and Ocean Sciences, University of Alaska Fairbanks, Fairbanks, Alaska, USA

[4]Division of Environment and Department of Mathematics, Hong Kong University of Science and Technology, Kowloon, Hong Kong, China

[†]Present address: GEOMAR | Helmholtz Center for Ocean Research Kiel, Kiel, Germany

*Corresponding author:

Dr. Minhan Dai

State Key Laboratory of Marine Environmental Science

Xiamen University

Xiang'an District

Xiamen 361102, China

Phone: +86-592-2182132

Fax: +86-592-2184101

E-mail: mdai@xmu.edu.cn

Abstract

It is generally known that the interplay between the carbon and nutrients supplied from subsurface waters via biological metabolism determines the CO_2 fluxes in upwelling systems. However, quantificational assessment of such interplay is difficult because of the dynamic nature of both upwelling circulation and the associated biogeochemistry. We recently proposed a new framework, the Ocean-dominated Margin (OceMar), for semi-quantitatively diagnosing the CO_2 source/sink nature of an ocean margin, highlighting that the relative consumption between carbon and nutrients determines if carbon is in excess (i.e., CO_2 source) or in deficit (i.e., CO_2 sink) in the upper waters of ocean margins relative to their off-site inputs from the adjacent open ocean. In the present study, such a diagnostic approach based upon both couplings of physics-biogeochemistry and carbon-nutrients was applied to resolve the CO_2 fluxes in the well-known upwelling system in the US west coast off Oregon and northern California, using data collected along three cross-shelf transects from the inner shelf to the open basin in spring/early summer 2007. Through examining the biological consumption on top of the water mass mixing revealed by the total alkalinity-salinity relationship, we successfully predicted and semi-analytically resolved the CO_2 fluxes showing strong uptake from the atmosphere beyond the nearshore regions. This CO_2 sink nature primarily resulted from the higher utilization of nutrients relative to dissolved inorganic carbon (DIC) based on their concurrent inputs from the depth. On the other hand, the biological responses to intensified upwelling were minor in nearshore waters off the Oregon-California coast, where significant CO_2 outgassing was observed and resolving CO_2 fluxes could be simplified without considering DIC/nutrient consumption, i.e., decoupling between upwelling and biological consumption. We reasoned that coupling physics and

biogeochemistry in the OceMar model would assume a steady state with balanced DIC and nutrients via both physical transport and biological alterations in comparable timescales.

1 Introduction

The contemporary coastal ocean, characterized by high primary productivity due primarily to the abundant nutrient inputs from both river plumes and coastal upwelling, is generally seen as a significant CO_2 sink at the global scale (Borges et al., 2005; Cai et al., 2006; Chen and Borges, 2009; Laruelle et al., 2010; Borges, 2011; Cai, 2011; Dai et al., 2013). However, mechanistic understanding of the coastal ocean carbon cycle remains limited, leading to the unanswered question of why some coastal systems are sources while others are sinks of atmospheric CO_2 in a given time scale. We recently proposed a new framework, the Ocean-dominated Margin (OceMar), for better shaping the concept of a coastal ocean carbon study (Dai et al., 2013). This framework highlights the importance of the boundary process between the open ocean and the ocean margin, and proposes a semi-analytical diagnostic approach to resolve sea-air CO_2 fluxes. The approach invokes an establishment of the water mass mixing scheme in order to define the physical transport, or the conservative portion of carbon and nutrients from the adjacent open ocean; and the constraint of the biogeochemical alteration of these non-local inputs in the upper waters of ocean margins. The water mass mixing scheme is typically revealed using conservative chemical tracers such as total alkalinity (TAlk) and/or dissolved calcium ions (Ca^{2+}) to bypass the identification of end-members associated with individual water masses that often possess high complexity in any given oceanic regime. The constraint of the biogeochemical alteration can then be estimated as the difference between the predicted values based on conservative mixing between end-members and the field measured values. The relative consumption between dissolved inorganic carbon (DIC) and nutrients determines if DIC is in excess or in deficit relative to the off-site input. Such excess DIC will eventually be released to the atmosphere through air-sea CO_2 exchange. Using two large marginal seas, the South China Sea (SCS) and

68 the Caribbean Sea (CS) as examples, we have successfully predicted, via evaluating DIC and
69 nutrient mass balance, the CO_2 outgassing that is consistent with field observations (Dai et al.,
70 2013). However, the OceMar concept and the diagnostic approach have not been verified on
71 upwelling systems that can be either sources (e.g., Friederich et al., 2002; Torres et al., 2003;
72 Fransson et al., 2006) or sinks (e.g., Borges et al., 2002; Santana-Casiano et al., 2009; Evans et
73 al., 2012) of atmospheric CO_2. While it is generally known that the interplay between the
74 nutrients and DIC supplied from subsurface waters via biological metabolism would determine
75 the CO_2 fluxes in upwelling systems, quantificational assessment of such interplay is difficult
76 because of the dynamic nature of both upwelling circulation and the associated biogeochemistry.
77 Our study therefore chose the upwelling system in the US west coast off Oregon and northern
78 California, to examine the CO_2 flux dynamics through our proposed mass balance approach
79 associated with carbon/nutrient coupling. The system under study is part of the eastern boundary
80 current in the North Pacific (Fig. 1). While strong equatorward winds in spring/summer drive
81 offshore Ekman transport at the surface over the coastal waters, the carbon and nutrient-rich deep
82 water is transported shoreward and upward over the shelf to compensate for the offshore
83 transport in the surface layer (Huyer, 1983; Kosro et al., 1991; Allen et al., 1995; Federiuk and
84 Allen, 1995; Gan and Allen, 2002). Outcrops of waters from depths of 150-200 m are frequently
85 observed in the nearshore on the Oregon-California shelf, where the surface partial pressure of
86 CO_2 (pCO_2) can reach levels near 1000 μatm. This water is then transported seaward and
87 southward while the pCO_2 is drawn down by biological productivity, and can be down to levels
88 of ~200 μatm, far below the atmospheric pCO_2 value (Hales et al., 2005, 2012; Feely et al., 2008;
89 Evans et al., 2011). Such a dramatic decrease in seawater pCO_2 may be due to the fact that the
90 complete utilization of the preformed nutrients in upwelled waters exceeds their corresponding

net DIC consumption, leading to the area off Oregon and northern California acting as a net sink of atmospheric CO_2 during the upwelling season (Hales et al., 2005, 2012). On the other hand, Evans et al. (2011) suggest that the spring/early summer undersaturated pCO_2 conditions in some offshore areas result from non-local productivity associated with the Columbia River (CR) plume, which transports ~77% of the total runoff from the western North America to the Pacific Ocean (Hickey, 1989).

In this context, the Oregon-California shelf in the upwelling season can be a potential OceMar-type system with the majority of DIC and nutrients in the upper layer originating from the non-local deep waters of the eastern North Pacific (eNP), though riverine inputs might complicate the application of the OceMar framework. On the other hand, the upper waters in offshore areas beyond the upwelling circulation on the Oregon-California shelf would be largely fed by on-site deep waters via vertical mixing, with minor influence of the CR plume.

2 Study area and data source

2.1 California Current system and upwelling circulation

The upwelling circulation off Oregon and northern California is linked with the eastern boundary current, the California Current (CC) occupying the open basin of the eNP (Barth et al., 2000). The CC is a broad and weak surface current (0-200 m) which carries low-salinity/temperature water equatorward from the subarctic Pacific (Lynn and Simpson, 1987). The deeper-lying California Undercurrent (CUC, 150-300 m), which has relatively high salinity and temperature, originates in the eastern Equatorial Pacific and flows poleward inshore along the west coast of North America (Thomson and Krassovski, 2010). The CC system is characterized by coastal upwelling in spring/summer, during which waters primarily composed

of the CC are transported upward from the depths of 150-200 m towards the nearshore surface off the Oregon-California coast (Castro et al., 2001).

Both field observations and modeling studies (Oke et al., 2002; Gan and Allen, 2005) show that the upwelling circulation pattern in the study area differs significantly between north and south of Newport (Fig. 1). North of Newport between 45.0 and 45.5°N with a relatively straight coastline and narrow shelf, the along-shore uniform bottom topography generally results in typical upwelling circulation with a southward coastal jet close to shore at Cascade Head (Fig. 1). Over the central Oregon shelf between 43.5 and 45.0°N, the highly variable bottom topography over Heceta Bank (Fig. 1) largely influences the upwelling circulation, leading to a complex three-dimensional flow pattern with offshore shifting of the coastal jet and development of northward flow inshore. At the coast along the southern part of Oregon and northern California between 39.0 and 43.0°N, an enhancement of coastal upwelling, jet separation and eddy formation are observed to be associated with interactions of the wind-forced coastal currents with Cape Blanco (Fig. 1) (Barth et al., 1998; Gan and Allen, 2005, and references therein).

2.2 Data source

Our data sets were based on the online published carbonate system and nutrient data collected along three transects off Oregon and northern California during the first North American Carbon Program (NACP) West Coast Cruise in spring/early summer 2007 (http://cdiac.ornl.gov/oceans/Coastal/NACP_West.html; Feely et al., 2008; Feely and Sabine, 2011). Transect 4 (stations 25-33 from nearshore to offshore) is located off Newport, Oregon. Transect 5 (stations 41-35 from nearshore to offshore) is located off Crescent City near the Oregon-California border. Transects 6 (stations 42-49 from nearshore to offshore) is located off Cape Mendocino, California. The most offshore stations on all transects were located in the open

basin of the eNP (Fig. 1).

3 Results and discussion

The region under study is highly dynamic potentially involving coastal upwelling, the CR plume and pelagic waters mixed by various Pacific water masses (Hill and Wheeler, 2002). Instead of accounting for all of the water masses contributing to the CC system, the mixing scheme in the upper waters along the three transects was examined via the total alkalinity-salinity (TAlk-Sal) relationship obtained during the sampling period so as to quantify the conservative portion of DIC and nitrate (NO_3). The end-members were therefore identified under this relationship, which might have experienced physical or biological alterations from their original water masses such as the CR and the CC. Subsequently, the biologically consumed DIC and NO_3 were quantified as the difference between their conservative values predicted from the derived end-member mixing and the corresponding field measurements. Finally, the CO_2 source/sink nature of the upper waters off Oregon and northern California was diagnosed via a mass balance approach by estimating the relative consumption between DIC and NO_3 and a simple sensitivity analysis was performed to test the robustness of the approach.

3.1 TAlk-Sal relationship

3.1.1 Through the entire water column off Oregon and northern California

Three generally linear relationships between TAlk and salinity were observed through the entire water column along Transect 4 (Fig. 2a). The first one was for waters with salinity lower than ~32.0 (corresponding to a depth of ~15-25 m), which were significantly influenced by the CR plume. The second one was for waters composed primarily of the CC with salinity between ~32.0 and ~33.9, including those immediately below the top buoyant layer at stations 26-32 and the surface waters at the outermost station 33 (Fig. 1). The higher-end salinity value of ~33.9

corresponded to a depth range of ~75-175 m, composed possibly of the upwelled high-salinity CUC waters. At station 27 (water depth ~170 m) for instance, salinity at depths of ~130 m and ~160 m reached ~34.0 with TAlk values of ~2260 μmol kg^{-1}, which were even higher than those of offshore waters at ~175 m (~2250 μmol kg^{-1}). These two data points were thus located on the third linear relationship for waters with salinity higher than ~33.9, the slope of which became much steeper, mainly reflecting the mixing between the approaching CUC and deep waters of the eNP (Fig. 2a).

All salinity values, including surface samples on Transects 5 and 6, were higher than 32.0 (Fig. 2b and 2c). With minor influence of the CR plume, the TAlk-Sal relationship displayed two generally linear phases through the entire water column along both transects, while the TAlk/salinity endpoints of each were comparable to those of the latter two observed on Transect 4. Note that the turning point with salinity of ~33.9 corresponded to a wider depth range of ~5-175 m (Fig. 2b and 2c), resulting from the most intensive upwelling on Transects 5 and 6 bringing deep waters to the nearshore surface (Feely et al., 2008).

As suggested by the generally linear TAlk-Sal relationships, surface waters beyond the CR plume and waters immediately below the top buoyant layer were directly linked to the underlying waters to the depth of ~175 m. We thus took a closer look at the TAlk-Sal relationship in the upper 175 m waters off Oregon and northern California.

3.1.2 In the upper 175 m waters off Oregon and northern California

In the upper 175 m waters along Transect 4, the linear regression for waters with salinity lower than ~32.0 had an intercept of ~1200 μmol kg^{-1}. This value agreed well with the observed TAlk of ~1000 μmol kg^{-1} in the main stream of the CR (Park et al., 1969b; Evans et al., 2013). The other linear regression for waters with salinity between ~32.0 and ~33.9 had a smaller

intercept of ~500 μmol kg^{-1}, implying a smaller contribution from the CR plume (Fig. 3a). Exceptions were observed at the shallowest station 25 (water depth ~50 m) and the deepest station 33 (water depth ~2900 m). The TAlk-Sal relationship completely followed the second phase for the upper 175 m waters at station 33 (Fig. 3a), suggesting a small fraction of the CR plume even in the surface waters of this outermost station on Transect 4. On the other hand, data points of the two variables were not well correlated through the entire water column of station 25 and fell off both regression lines (Fig. 3a). The water mass mixing at this innermost station was not as straightforward, despite minor freshwater admixture as suggested by the high surface salinity of >32.0.

The TAlk-Sal relationship in the upper 175 m waters on Transects 5 and 6 displayed two similar phases. One was the linear regression for stations 35-38 (deeper than ~800 m) and stations 45-49 (deeper than ~1400 m), with slope and intercept values comparable to the second phase observed on Transect 4. The other was the linear regression for the three shallow stations on both transects largely influenced by coastal upwelling (Feely et al., 2008) (Fig. 3b and 3c). This phase was not clearly seen from the full TAlk-Sal plot (Fig. 2b and 2c), as the salinity in the upper 175 m waters at stations 39 and 44 as well as in the entire water column of stations 40-43 varied within a much smaller range of ~33.3-~34.0. The negligible intercepts of this TAlk-Sal regression suggested insignificant freshwater input with zero solutes to the intensive upwelling zone off Oregon and northern California (Fig. 3b and 3c).

All phases shown in Fig. 3 displayed good linear TAlk-Sal relationships ($r>0.94$), indicating an overall two end-member mixing scheme for each phase. Although the non-conservativity of TAlk existed, it was not that significant as seen by the deviations of a few data points from each linear regression (Fig. 3). As a matter of fact, Fassbender et al. (2011) estimate that the

contribution from $CaCO_3$ dissolution to the TAlk addition in the surface mixed layer on Transect 5 was <10 μmol kg^{-1} (<0.5% of their absolute contents in seawater) and well around the analytical precision. Such small non-conservative portions would not compromise the application of TAlk as a conservative tracer. Note that the two end-member mixing was not spatially homogeneous in the upper waters off Oregon and northern California during the sampling period. The top waters at stations 26-32 on Transect 4 were imprinted by the CR plume with a salinity around ~30.0. During the transport from the mouth of the CR estuary, the plume water increasingly mixed with adjacent oceanic waters, largely feeding its pathway. However, the majority of DIC and nutrients in waters immediately below the buoyant layer, as well as in surface waters at station 33 and possibly at station 25, originated from deep waters through coastal upwelling and/or vertical mixing. The influence of the CR plume still occurred but was diluted by other freshwater masses such as rainwater, suggesting a mixing scheme between the deep water of the eNP and a combined freshwater end-member (Park, 1966;- 1968). Such mixing was also applicable to the surface waters at stations 35-38 on Transect 5 and stations 45-49 on Transect 6. On the other hand, the upper 175 m waters or the entire water column at stations 39-44 resulted from a simple two end-member mixing between the upwelling source water and the rainwater with zero solutes, establishing for them an apparent OceMar-type system.

3.2 ΔDIC and ΔNO_3 in the upper waters off Oregon and northern California

The defined mixing schemes enabled us to estimate the non-conservative portion of DIC (ΔDIC) and NO_3 (ΔNO_3) in the upper waters off Oregon and northern California following Dai et al. (2013):

$$\Delta DIC = DIC^{cons} - DIC^{meas} \quad (1)$$

$$\Delta NO_3 = NO_3^{cons} - NO_3^{meas} \quad (2)$$

$$X^{cons} = \frac{Sal^{meas}}{Sal^{ref}} \times (X^{ref} - X^{eff}) + X^{eff} \quad (3)$$

The superscripts "cons" and "meas" in Eqs (1) and (2) denote conservative-mixing induced and field measured values. In Eq. (3), X represents DIC or NO_3 while Sal^{meas} is the CTD measured salinity. Sal^{ref} and X^{ref} are the reference salinity and concentration of DIC or NO_3 for the deep water end-member, which are the averages of all ~175 m samples from stations involved in each mixing scheme. Specifically, for waters immediately below the top buoyant layer at stations 27-32 and waters in the surface mixed layer at stations 25 and 33 on Transect 4, the deep water end-member values of the reference salinity and concentrations of DIC or NO_3 were the averages of ~175 m samples from stations 28-33 (Fig. 1). On Transects 5 and 6, the preformed salinity, DIC and NO_3 values for waters in the surface mixed layer at stations 35-38 and at stations 45-49 were the averages of ~175 m samples of these stations. For the upper waters influenced by the intensified upwelling at stations 39-41 and stations 42-44, the deep water end-member was selected as the ~175 m water at station 39 and at station 44 (Fig. 1).

The X^{eff} in Eq. (3) denotes the effective concentration of DIC or NO_3 sourced from the freshwater input to various zones off Oregon and northern California. Since rainwater was assumed to have no solutes, both DIC^{eff} and NO_3^{eff} would be zero for waters in the surface mixed layer of stations 39-41 on Transect 5 and stations 42-44 on Transect 6. On the other hand, the estimation of X^{eff} associated with the CR followed the method for the OceMar case study of the CS, which has a noticeable DIC^{eff} from the combination of the Amazon River and the Orinoco River (Dai et al., 2013).

Since bicarbonate dominates other CO_2 species and other alkalinity components, DIC concentrations in the main stream of the CR are numerically similar to TAlk, which are also around ~1000 μmol kg^{-1} (Park et al., 1969a, 1970). This value was taken as the DIC end-member

of the CR. The NO_3 end-member value was selected as 15 μmol kg^{-1} based on recent years' observations in May and July at station SATURN-05 established in the upstream CR (database of the Center for Coastal Margin Observation and Prediction; http://www.stccmop.org/datamart/observation_network/fixedstation?id=saturn05#anchor_5). Assuming that the biological consumption of DIC and NO_3 in the CR plume followed the Redfield ratio (Redfield et al., 1963), the DIC removal was estimated to be ~100 μmol kg^{-1} (approximately 15·106/16), while NO_3 was rapidly consumed along the pathway of the CR plume and generally depleted in the area beyond the plume (Aguilar-Islas and Bruland, 2006; Lohan and Bruland, 2006). As a consequence, the complete DIC^{eff} and NO_3^{eff} in the upper waters from the CR would be ~900 μmol kg^{-1} and ~0 μmol kg^{-1}.

If the combined freshwater end-member was a mixture of the CR and the rainwater with zero solutes, the intercept values of 521.0±30.6 (Fig. 3a), 677.4±32.2 (Fig. 3b) and 609.9±34.1 (Fig. 3c) derived from the TAlk-Sal regression indicated that the CR fractions were ~50, ~65 and ~60% (approximately 500/1000, 650/1000 and 600/1000 taking ~1000 μmol kg^{-1} as the TAlk end-member value of the CR, Park et al., 1969b; Evans et al., 2013). The DIC^{eff} from the freshwater input was thus estimated to be ~450 μmol kg^{-1} (approximately 900·50%) for waters immediately below the top buoyant layer at stations 27-32 and waters in the surface mixed layer at stations 25 and 33 on Transect 4, which was slightly lower than the ~585 μmol kg^{-1} (approximately 900·65%) and the ~540 μmol kg^{-1} (approximately 900·60%) for waters in the surface mixed layer at stations 35-38 on Transect 5 and at stations 45-49 on Transect 6, respectively. The NO_3^{eff} in any combined freshwater end-member was zero.

Note that numerous small mountainous rivers are distributed on the Oregon-California coast, which might also have diluted the CR plume inducing the lower intercept of the TAlk-Sal

regression observed on the three transects (Fig. 3). The average wintertime discharge from these Coast Range rivers is estimated to be ~2570 m^3 s^{-1} (Wetz et al., 2006), which is more than an order of magnitude higher than that in the summer (Colbert and McManus, 2003; Sigleo and Frick, 2003). However, the CR discharge in May to June 2007 reached its maximum of ~15000 m^3 s^{-1} (Evans et al., 2013), which should be approximately two orders of magnitude higher than the discharge of small rivers. This significant contrast would suggest that inputs from small rivers should be negligible compared to the CR plume. In particular, inputs from small rivers are normally restricted to a narrow band near the coast, whereas the research domain of this study extended to the open basin of the eNP. Even the surface salinity at the innermost stations (i.e., station 25 on Transect 4, station 41 on Transect 5 and station 42 on Transect 6; Fig. 1) was as high as ~32.5, ~33.9 and ~34.0, which would rule out the influence of small rivers.

3.3 Evaluating the CO_2 source/sink nature in the upper waters off Oregon and northern California

The coupling of DIC and NO_3 dynamics could then be examined based on the classic Redfield ratio of C:N=106:16=6.6 (Redfield et al., 1963). Positive values of the difference between ΔDIC and 6.6ΔNO_3 (ΔDIC−6.6ΔNO_3) suggested a CO_2 source term since "excess ΔDIC" was removed by CO_2 degassing into the atmosphere. In contrast, negative ΔDIC−6.6ΔNO_3 suggested that "deficient ΔDIC" was supplied via the atmospheric CO_2 input to the ocean representing a CO_2 sink. Such net CO_2 exchange between the seawater and the atmosphere was further quantified as the sea-air difference of pCO_2 (ΔpCO_2) via the Revelle factor (RF), which is referred to as the fractional change in seawater CO_2 over that of DIC at a given temperature, salinity and alkalinity and indicates the ocean's sensitivity to an increase in atmospheric CO_2 (Revelle and Suess, 1957;

Sundquist et al., 1979). Because pCO_2 and CO_2 are proportional to each other, the RF can be illustrated as:

$$RF = \frac{\partial pCO_2 / pCO_2}{\partial DIC / DIC} \quad (4)$$

Here, ∂pCO_2 and ∂DIC are the fractional changes of pCO_2 and DIC in the surface seawater. In the OceMar framework, ∂DIC equals $\Delta DIC - 6.6\Delta NO_3$ that is solely achieved through air-sea CO_2 exchange, implying that ∂pCO_2 represents the sea-air ΔpCO_2. Given an initial balance of CO_2 between the seawater and the atmosphere, the sea-air ΔpCO_2 is obtained by:

$$Sea\text{-}air\ \Delta pCO_2 = \partial pCO_2 = RF \times pCO_2 \times \frac{\partial DIC}{DIC} = RF \times pCO_2^{air} \times \frac{\Delta DIC - 6.6\Delta NO_3}{DIC} \quad (5)$$

As shown in Fig. 4, the estimated $\Delta DIC - 6.6\Delta NO_3$ values and their corresponding sea-air ΔpCO_2 in the upper waters off Oregon and northern California were overall below zero, suggesting a significant CO_2 sink nature.

3.3.1 Transect 4

On Transect 4 off Newport, the average value of $\Delta DIC - 6.6\Delta NO_3$ was −23±2 μmol kg^{-1} in waters immediately below the top buoyant layer at stations 27-32, which equaled the average value for the surface mixed layer at station 33 (Fig. 4a). Note that we were not able to derive values of $\Delta DIC - 6.6\Delta NO_3$ at station 26 where NO_3 data were not available. Although located at different depths, the two water parcels experienced similar physical mixing and biogeochemical modifications inducing the same CO_2 signature. The former water mass should work as a CO_2 sink when in contact with the atmosphere before or after the passage of the episodic CR plume. The average sea-air ΔpCO_2 resulting from the combined deficient ΔDIC was −54±4 μatm (Fig. 3a). Given the atmospheric pCO_2 of ~390 μatm (Evans et al., 2011), the seawater pCO_2 in these regions was thus estimated to be 336±4 μatm, which agreed rather well with the field

318 measurements of 334±13 μatm (the underway seawater pCO_2 data were not available online but
319 alternatively calculated by applying TAlk and DIC data into the CO2SYS program, Lewis and
320 Wallace, 1998).

321 The diagnostic approach was not applied to the top buoyant layer since the aged CR plume
322 might have experienced complex mixing with various surrounding water masses during its
323 transport, as indicated by the scatter TAlk-Sal relationship (Fig. 3a). However, the far-field CR
324 plume is suggested to be a strong sink of atmospheric CO_2 due to earlier biological consumption
325 (Evans et al., 2011), which was supported by the observed low pCO_2 of ~220-300 μatm in the
326 top buoyant layer on Transect 4. As a consequence, the CO_2 sink nature in the upper waters from
327 the outer shelf (the bottom depth of station 27 was ~170 m) to the open basin off Newport,
328 Oregon would primarily result from the higher utilization of nutrients relative to DIC based on
329 their concurrent inputs from deep waters. The non-local high productivity in the CR plume could
330 inject even lower pCO_2 but this effect would be transitory.

331 At the innermost station 25 on Transect 4, highly positive values of $\Delta DIC - 6.6\Delta NO_3$ and sea-
332 air ΔpCO_2 (~82 μmol kg^{-1} and ~157 μatm, respectively) were obtained for the surface mixed
333 layer of this station, indicating a significant CO_2 source. However, the lowest pCO_2 value of
334 ~170 μatm was observed in these nearshore waters off Oregon. The poor correlation between
335 TAlk and salinity at station 25 (Fig. 3a) might compromise the estimation, whereas the same
336 method (Eqs 1-5) was successfully applied to other stations on Transect 4 with a distinct TAlk-
337 Sal relationship (i.e., the second phase in Fig. 3a). Note that coastal upwelling clearly influenced
338 the bottom water at station 25 as indicated by the comparable salinity and TAlk values to those in
339 offshore 200 m waters. Instead of being fed by the upwelled deep water, the DIC and nutrients in
340 the surface mixed layer might have originated from horizontal admixture of the surrounding

waters. These waters possibly experienced intense diatom blooms due to the fact that the surface silicate concentrations at station 25 were almost zero, which led to the most undersaturated pCO_2 condition observed in the upper waters off Oregon.

3.3.2 Transects 5 and 6

On Transect 5 near the Oregon-California border, the average $\Delta DIC - 6.6\Delta NO_3$ and sea-air ΔpCO_2 were estimated to be −20±3 μmol kg^{-1} and −48±8 μatm in the surface mixed layer of stations 35-38 (Fig. 4b). Both values were comparable to those obtained from the surface mixed layer of stations 45-49 on Transect 6 (−23±3 μmol kg^{-1} and −53±6 μatm, respectively; Fig. 4c) and on Transect 4, indicating a similar magnitude of the CO_2 sink term in offshore areas along the Oregon and northern California coast. The estimated sea surface pCO_2 of 342±8 μatm for Transect 5 and 337±6 μatm for Transect 6 were consistent with the field measurements of 332±12 and 346±12 μatm in these regions.

The diagnosed CO_2 flux in the nearshore was also comparable between Transects 5 and 6. The $\Delta DIC - 6.6\Delta NO_3$ and sea-air ΔpCO_2 in the surface mixed layer of stations 39-44, although still below zero, were obviously higher than those of stations 35-38 on Transect 5 and of stations 45-49 on Transect 6 (Fig. 4b and 4c). Such an increase was expected since stations 39-44 were located in the area with the most intensive upwelling, which brought CO_2-rich deep waters to the nearshore surface (Feely et al., 2008). However, our estimation suggested a weaker CO_2 sink or close to being in equilibrium with the combined estimated sea surface pCO_2 of 368±14 μatm, whereas the field measurements of ~600-1000 μatm indicated that the coastal upwelling zone should be a very strong source of CO_2 to the atmosphere.

Therefore, we took a closer look at Transect 5: A uniform salinity of ~34.0 through the entire water column was observed at stations 40 and 41 due to the outcrop of the upwelling source

water at the surface of the inner shelf on Transect 5 (Feely et al., 2008). Although salinity in the surface mixed layer at station 39 was lower, around ~33.4, the dilution effect of rainwater should be negligible. After removing the rainwater from the mixing scheme and calculating ΔDIC and ΔNO_3 by directly subtracting the field observed value from the end-member value for the upwelling source water (Eqs 6 and 7; DIC^{ref} and NO_3^{ref} were field measurements of ~200 m water samples at station 39), the $\Delta DIC - 6.6\Delta NO_3$ values were rapidly increased to above zero in the surface mixed layer at stations 39 and 40, while values at station 41 with a small increase were still overall below zero (Fig. 5a). Correspondingly, the estimated sea surface pCO_2 values were higher than the atmospheric CO_2 value at stations 39 and 40 while they were slightly lower than that at station 41. However, these values still largely fell below the field measurements of seawater pCO_2, displaying shoreward increasing differences from ~200 to ~700 μatm (Fig. 5b).

$$\Delta DIC = DIC^{ref} - DIC^{meas} \quad (6)$$

$$\Delta NO_3 = NO_3^{ref} - NO_3^{meas} \quad (7)$$

With or without taking rainwater into account, our diagnostic approach did not work in the nearshore with strong upwelling off Oregon and northern California, even though the mixing scheme of this region was in accordance with the OceMar concept. We contend that OceMar assumes a steady state with balanced DIC and nutrients via both physical mixing and biological alterations in comparable timescales. However, the continuous inputs from the coastal upwelling might have led to the accumulation of DIC and nutrients in the nearshore surface, which could not be timely consumed by the phytoplankton community, suggesting a possible non-steady state. Fassbender et al. (2011) estimate that the age of the surface mixed layer at nearshore stations on Transect 5 is only ~0.2 days, during which the DIC and NO_3 consumption via organic carbon production was almost zero and $CaCO_3$ dissolution contributed a small fraction to the

slightly elevated DIC in the upwelled waters. They further predict that the nearshore surface pCO_2 on Transect 5 will decrease to levels of ~200 μatm in ~30 days until NO_3 exhaustion via continued biological productivity, implying the achievement of a steady state (Fassbender et al., 2011). Minor biological responses during the intensified upwelling period were also observed in summer 2008, allowing highly oversaturated pCO_2 surface water to persist on the inner shelf off Oregon for nearly two months (Evans et al., 2011). At this point, it is uncertain why there was such a prolonged delay from the phytoplankton community to the persistent source of upwelled DIC and nutrients. Note that under the condition of a more prevailing upwelling-favorable wind as a predicted consequence of climate change (e.g., Snyder et al., 2003; Diffenbaugh et al., 2004; Sydeman et al., 2014), the nearshore waters off the Oregon-California coast in the upwelling season might always be in a non-steady state, and it is expected that fewer periodic relaxation events or reversals would further decrease the chance for the biological response to be factored in.

In addition, the negligible biological consumption might involve large errors when calculating Δ. The portion of ΔDIC and ΔNO_3 at station 41 relative to the preformed values of the upwelling source water were only ~0.5 and ~10%, slightly higher than the measurement uncertainties. The portion of DIC and NO_3 consumption in the surface mixed layer at offshore stations on Transect 5 were, however, one order of magnitude higher (~7 and ~90%, respectively). This contrast might partially explain why the OceMar framework did not work when insignificant biological alterations occurred. Given the predominant control of physical mixing, we contend that the prediction of the CO_2 flux in the nearshore off Oregon and northern California with intensified upwelling could be simplified without considering DIC/nutrient consumption. In other words,

surface CO_2 levels in this region were simply imprints of the upwelling source water (pCO_2 ~1000 μatm at ~150-200 m) with minor dilution by rainwater.

3.4 Sensitivity analysis

In the above exercise, both the end-member values revealed in the water mass mixing scheme and the Redfield ratio adopted in coupling DIC and nutrients were critically important in resolving the CO_2 fluxes. We thus conducted sensitivity analysis for these two sets of variables for the CO_2 sink zones off Oregon and northern California where our diagnostic approach worked well (i.e., waters immediately below the top buoyant layer at stations 27-32 as well as waters in the surface mixed layer at station 33 on Transect 4, waters in the surface mixed layer at stations 35-38 on Transect 5 and waters in the surface mixed layer at stations 45-49 on Transect 6).

3.4.1 The combined freshwater end-member

While the value of ~1000 μmol kg^{-1} was selected for TAlk and DIC in the main stream of the CR, the field observed TAlk varies within a range of ~800-1200 μmol kg^{-1} in spring/early summer (Evans et al., 2013). We thus took the values of ~800 and ~1200 μmol kg^{-1} as the lower and upper limit of the TAlk and DIC end-members in the CR to test the diagnostic approach. Following the same calculation of the combined freshwater end-member (X^{eff} in Eq. 3), the lower and upper limit of DIC^{eff} was estimated to be ~435 and ~460 μmol kg^{-1}, for waters immediately below the top buoyant layer at stations 27-32 and in the surface mixed layer at station 33 on Transect 4. Those values were ~565 and ~600 μmol kg^{-1} for waters in the surface mixed layer at stations 35-38 on Transect 5, and ~520 and ~550 μmol kg^{-1} in the surface mixed layer at stations 45-49 on Transect 6. The NO_3^{eff} in any scenario was still zero.

The newly diagnosed $\Delta DIC - 6.6\Delta NO_3$ and sea-air ΔpCO_2 on Transects 4, 5 and 6 displayed no difference with those with the initial TAlk and DIC of ~1000 μmol kg^{-1} in the CR (Table 1), while all estimated sea surface pCO_2 values were within error compared to the field measurements. Although the TAlk and DIC end-members had large variations of up to ~400 μmol kg^{-1} in the main stream of the CR, the corresponding range of DIC^{eff} contributing to waters beyond the CR plume significantly decreased by approximately one order of magnitude, implying minor influence of its variations on our diagnostic of the CO_2 fluxes.

3.4.2 The deep water end-member

We selected values at ~175 m as the deep water end-member based on the TAlk-Sal relationship, whereas this end-member depth might not be spatially stable in a highly dynamic upwelling system. Previous studies also show that the upwelling source water onto the Oregon-California shelf can vary between 150 and 200 m (e.g., Hales et al., 2005; Feely et al., 2008). We thus tested the diagnostic approach with values at three other depths of ~130, ~150 and ~200 m.

On Transects 4 and 6, the newly estimated $\Delta DIC - 6.6\Delta NO_3$, sea-air ΔpCO_2 and sea surface pCO_2 using end-member values at both ~150 and ~200 m agreed well with those using end-member values at ~175 m, while the three variables were slightly higher using end-member values at ~130 m (Table 2). On Transect 5, the newly estimated $\Delta DIC - 6.6\Delta NO_3$, sea-air ΔpCO_2 and sea surface pCO_2 using end-member values at both ~130 and ~150 m agreed well with those using end-member values at ~175 m, while the three variables were slightly higher using end-member values at ~200 m (Table 2).

3.4.3 The C/N uptake ratio

In a given oceanic setting, the real C/N uptake ratio during organic carbon production can be different from the Redfield one of ~6.6 (Redfield et al., 1963). For instance, higher ratios

454 estimated from the DIC-NO_3 relationship are observed in both coastal waters and open ocean
455 sites, possibly resulting from excess DIC uptake via the production of dissolved organic carbon
456 (Sambrotto et al., 1993; Ianson et al., 2003). However, since the precise estimation of the C/N
457 uptake ratio (via e.g. in situ incubation experiments) is still problematic, such data are currently
458 scarce over the world's oceans and the empirical stoichiometry is routinely applied into field
459 studies investigating the dynamics and coupling of carbon and nutrients (e.g., Chen et al., 2008;
460 Fassbender et al., 2011). Fassbender et al. (2011) apply another empirical C/N uptake ratio of 7.3
461 (approximately 117/16; Anderson and Sarmiento, 1994) into the same data set as this study. We
462 thus performed a simple sensitivity analysis using this alternative value of 7.3, which implies
463 excess DIC uptake relative to NO_3.

464 Since $\Delta DIC - 7.3\Delta NO_3$ values were obviously smaller than $\Delta DIC - 6.6\Delta NO_3$ ones, the new sea-
465 air ΔpCO_2 values were halved (Table 3). Correspondingly, the newly estimated sea surface pCO_2
466 values on Transects 4, 5 and 6 were ~35-45 μatm lower than the estimation using the Redfield
467 ratio, which were however consistent with the field measurements. Given that the Redfield ratio
468 also works in our OceMar case studies of the SCS and the CS (Dai et al., 2013), we contend that
469 this classic ratio could be preferentially employed if the field observed elemental stoichiometry
470 is not available. Moreover, as Martz et al. (2014) point out, "treating the Redfield ratios as global
471 or regional constants may be acceptable in the context of interpreting snapshots of the water
472 column captured in shipboard bottle data".

473 The above notion was also supported by examining the slope of the linear regression between
474 DIC and NO_3 normalized to a constant salinity in the surface water or in the surface mixed layer,
475 which provides an alternative to the C/N uptake ratio associated with organic carbon production
476 (Sambrotto et al., 1993; Wong et al., 2002; Ianson et al., 2003). Given a non-zero combined

freshwater end-member, we adopted in this study an approach of regional normalization (Friis et al., 2003; Cao et al., 2011) as:

$$nX = \frac{X^{meas} - X^{eff}}{Sal^{meas}} \times Sal^{aver} + X^{eff} \quad (8)$$

Here, nX and X^{meas} are salinity normalized and field measured values for DIC and NO_3. Sal^{meas} is the CTD measured salinity. Sal^{aver} is the average salinity value of ~33.0 in these CO_2 sink zones, which was selected as the constant salinity. X^{eff} is the same as that in Eq. (3), denoting the effective concentration of DIC or NO_3 sourced from the freshwater input to various zones off Oregon and northern California. While the NO_3^{eff} in any combined freshwater end-member was zero, the DIC^{eff} was ~450 μmol kg^{-1} for waters immediately below the top buoyant layer at stations 27-32 and waters in the surface mixed layer at stations 25 and 33 on Transect 4, ~585 μmol kg^{-1} for waters in the surface mixed layer at stations 35-38 on Transect 5, and ~540 μmol kg^{-1} for waters in the surface mixed layer at stations 45-49 on Transect 6.

As shown in Fig. 6, our new analysis with all data from the CO_2 sink zones along the three transects revealed a slope of 6.70±0.37. This value was within error comparable to that of 6.6, suggesting that using the Redfield ratio in our diagnostic approach was in order.

4 Concluding Remarks

The semi-analytical diagnostic approach of mass balance that couples physical transport and biogeochemical alterations was well applied to the CO_2 sink zones off Oregon and northern California, extending from the outer shelf to the open basin. In these zones with the absence of any significant influence of the CR plume, the source of DIC was largely from deep waters of the eNP and the ultimate CO_2 sink nature was determined by the higher nutrient consumption than DIC in the upper waters. On the other hand, the estimated CO_2 flux was opposite to the field observations in the coastal upwelling zone along the Oregon-California coast, which behaved

like a typical OceMar system in terms of its mixing process. This discrepancy was very likely due to minor biological responses during the intensified upwelling period, making our mass balance approach based on the coupled physical biogeochemistry invalid. This suggested that the applicability of the proposed semi-analytical diagnostic approach is limited to steady state systems with comparable timescales of water mass mixing and biogeochemical reactions. In such a physical mixing prevailing regime, resolving the CO_2 fluxes could be simplified without considering the biological consumption of DIC and nutrients. Further work is however needed to understand the carbon and nutrient dynamics as well as the timing between physics and biology associated with coastal upwelling.

509 *Acknowledgments.* This work was funded by the National Natural Science Foundation of China
510 through grants 91328202, 41121091, 90711005, and 41130857, and the National Basic Research
511 Program (973) sponsored by the Ministry of Science and Technology through grant
512 2009CB421200. We are very grateful to the Carbon Dioxide Information Analysis Center
513 (CDIAC; http://cdiac.ornl.gov/oceans/) for the online published data of the first North American
514 Carbon Program (NACP) West Coast Cruise. Zhimian Cao is supported by the Humboldt
515 Research Fellowship for postdoctoral researchers provided by the Alexander von Humboldt
516 Foundation. We thank John Hodgkiss for his help with English.

References

Aguilar-Islas, A. M., and Bruland, K. W.: Dissolved manganese and silicic acid in the Columbia River plume: A major source to the California current and coastal waters off Washington and Oregon, Mar. Chem., 101, 233-247, 2006.

Allen, J. S., Newberger, P. A., and Federiuk, J.: Upwelling circulation on the Oregon continental shelf. Part I: Response to idealized forcing, J. Phys. Oceanogr., 25, 1843-1866, 1995.

Anderson, L. A., and Sarmiento, J. L.: Redfield ratios of remineralization determined by nutrient data analysis, Global Biogeochem. Cycles, 8, 65-80, 1994.

Barth, J. A. and Smith, R. L.: Separation of a coastal upwelling jet at Cape Blanco, Oregon, USA, in: Benguela Dynamics: Impacts of Variability on Shelf-Sea Environments and their Living Resources, edited by S. C. Pillar, C. L. Moloney, A. I. L. Payne, and F. A. Shillington, S. Afr. J. Mar. Sci., 19, 5-14, 1998.

Barth, J. A., Pierce, S. D., and Smith, R. L.: A separating coastal upwelling jet at Cape Blanco, Oregon and its connection to the California Current System, Deep-Sea Res. II, 47, 783-810, 2000.

Borges, A. V.: Present day carbon dioxide fluxes in the coastal ocean and possible feedbacks under global change, in: Oceans and the Atmospheric Carbon Content, edited by P. Duarte, and J. M. Santana-Casiano, Springer Science+Business Media B.V., chap. 3, 47-77, 2011.

Borges, A. V., Delille, B., and Frankignoulle, M.: Budgeting sinks and sources of CO_2 in the coastal ocean: Diversity of ecosystems counts, Geophys. Res. Lett., 32, L14601, doi:10.1029/2005GL023053, 2005.

Borges, A. V., and Frankignoulle, M.: Distribution of surface carbon dioxide and air-sea exchange in the upwelling system off the Galician coast, Global Biogeochem. Cycles, 16,

1020, doi:10.1029/2000GB001385, 2002.

Cai, W.-J.: Estuarine and coastal ocean carbon paradox: CO_2 sinks or sites of terrestrial carbon incineration?, Annu. Rev. Mar. Sci., 3, 123-145, 2011.

Cai, W.-J., Dai, M., and Wang, Y.: Air-sea exchange of carbon dioxide in ocean margins: A province-based synthesis, Geophys. Res. Lett., 33, L12603, doi:10.1029/2006GL026219, 2006.

Cao, Z., Dai, M., Zheng, N., Wang, D., Li, Q., Zhai, W., Meng, F., and Gan, J.: Dynamics of the carbonate system in a large continental shelf system under the influence of both a river plume and coastal upwelling, J. Geophys. Res., 116, G02010, doi:10.1029/2010JG001596, 2011.

Castro, C. G., Chavez, F. P., and Collins, C. A.: Role of the California Undercurrent in the export of denitrified waters from the eastern tropical North Pacific, Global Biogeochem. Cycles, 15(4), 819-830, doi:10.1029/2000GB001324, 2001.

Chase, Z., Strutton, P. G., and Hales, B.: Iron links river runoff and shelf width to phytoplankton biomass along the U.S. West Coast, Geophys. Res. Lett., 34, L04607, doi:10.1029/2006GL028069, 2007.

Chen, C.-T. A., and Borges, A. V.: Reconciling opposing views on carbon cycling in the coastal ocean: Continental shelves as sinks and near-shore ecosystems as sources of atmospheric CO_2, Deep-Sea Res. II, 56, 578-590, 2009.

Chen, F., Cai, W.-J., Wang, Y., Rii, Y. M., Bidigare, R. R., and Benitez-Nelson, C. R.: The carbon dioxide system and net community production within a cyclonic eddy in the lee of Hawaii, Deep-Sea Res. II, 55, 1412-1425, 2008.

Colbert, D., and McManus, J.: Nutrient biogeochemistry in an upwelling-influenced estuary of

563 the Pacific Northwest (Tillamook Bay, Oregon, USA), Estuaries, 26, 1205-1219, 2003.
564 Dai, M., Cao, Z., Guo, X., Zhai, W., Liu, Z., Yin, Z., Xu, Y., Gan, J., Hu, J., and Du, C.: Why are
565 some marginal seas sources of atmospheric CO_2?, Geophys. Res. Lett., 40, 2154-2158,
566 doi:10.1002/grl.50390, 2013.
567 Diffenbaugh, N. S., Snyder, M. A., and Sloan, L. C.: Could CO_2-induced land-cover feedbacks
568 alter near-shore upwelling regimes?, Proc. Natl. Acad. Sci. USA, 101, 27-32, 2004.
569 Evans, W., Hales, B., and Strutton, P. G.: Seasonal cycle of surface ocean pCO_2 on the Oregon
570 shelf, J. Geophys. Res., 116, C05012, doi:10.1029/2010JC006625, 2011.
571 Evans, W., Hales, B., and Strutton, P. G.: pCO_2 distributions and air-water CO_2 fluxes in the
572 Columbia River estuary, Estuar. Coast. Shelf Sci., 117, 260-272, 2013.
573 Evans, W., Hales, B., Strutton, P. G., and Ianson, D.: Sea-air CO_2 fluxes in the western Canadian
574 coastal ocean, Prog. Oceanogr., 101, 78-91, 2012.
575 Fassbender, A. J., Sabine, C. L., Feely, R. A., Langdon, C., and Mordy, C. W.: Inorganic carbon
576 dynamics during northern California coastal upwelling, Cont. Shelf Res., 31, 1180-1192,
577 2011.
578 Federiuk, J., and Allen, J. S.: Upwelling circulation on the Oregon continental shelf. Part II:
579 Simulations and comparisons with observations, J. Phys. Oceanogr., 25, 1867-1889, 1995.
580 Feely, R., and Sabine, C.: Carbon dioxide and hydrographic measurements during the 2007
581 NACP West Coast Cruise,
582 http://cdiac.ornl.gov/ftp/oceans/NACP_West_Coast_Cruise_2007/, Carbon Dioxide
583 Information Analysis Center, Oak Ridge National Laboratory, US Department of Energy,
584 Oak Ridge, Tennessee, doi:
585 10.3334/CDIAC/otg.CLIVAR_NACP_West_Coast_Cruise_2007, 2011.

586 Feely, R. A., Sabine, C. L., Hernandez-Ayon, J. M., Ianson, D., and Hales, B.: Evidence for
587 upwelling of corrosive “acidified” water onto the continental shelf, Science, 320, 1490-1492,
588 2008.
589 Fransson, A., Chierici, M., and Nojiri, Y.: Increased net CO_2 outgassing in the upwelling region
590 of the southern Bering Sea in a period of variable marine climate between 1995 and 2001, J.
591 Geophys. Res., 111, C08008, doi:10.1029/2004JC002759, 2006.
592 Friederich, G. E., Walz, P. M., Burczynski, M. G., and Chavez, F. P.: Inorganic carbon in the
593 central California upwelling system during the 1997-1999 El Niño-La Niña event, Prog.
594 Oceanogr., 54, 185-203, 2002.
595 Friis, K., Körtzinger, A., and Wallace, D. W. R.: The salinity normalization of marine inorganic
596 carbon chemistry data, Geophys. Res. Lett., 30(2), 1085, doi:10.1029/2002GL015898, 2003.
597 Gan, J. and Allen, J. S.: A modeling study of shelf circulation off northern California in the
598 region of the Coastal Ocean Dynamics Experiment, response to relaxation of upwelling, J.
599 Geophys. Res., 107(C9), 3123, doi:10.1029/2000JC000768, 2002.
600 Gan, J., and Allen, J. S.: Modeling upwelling circulation off the Oregon coast, J. Geophys. Res.,
601 110, C10S07, doi:10.1029/2004JC002692, 2005.
602 Hales, B., Takahashi, T., and Bandstra, L.: Atmospheric CO_2 uptake by a coastal upwelling
603 system, Global Biogeochem. Cycles, 19, GB1009, doi:10.1029/2004GB002295, 2005.
604 Hales, B., Struttong, P. G., Saraceno, M., Letelier, R., Takahashi, T., Feely, R., Sabine, C., and
605 Chavez, F.: Satellite-based prediction of pCO_2 in coastal waters of the eastern North Pacific,
606 Prog. Oceanogr., 103, 1-15, 2012.
607 Hickey, B. M.: Patterns and processes of circulation over the Washington continental shelf and
608 slope, in: Coastal Oceanography of Washington and Oregon, Elsevier Sci., New York, 41-

115, doi:10.1016/S0422-9894(08)70346-5, 1989.

Hill, J. K., and Wheeler, P. A.: Organic carbon and nitrogen in the northern California current system: comparison of offshore, river plume, and coastally upwelled waters, Prog. Oceanogr., 53, 369-387, 2002.

Huyer, A.: Coastal upwelling in the California Current system, Prog. Oceanogr., 12, 259-284, 1983.

Ianson, D., Allen, S. E., Harris, S. L., Orians, K. J., Varela, D. E., and Wong, C. S.:The inorganic carbon system in the coastal upwelling region west of Vancouver Island, Canada, Deep-Sea Res. I, 50, 1023-1042, 2003.

Kosro, P. M., Huyer, A., Ramp, S. R., Smith, R. L., Chavez, F. P., Cowles, T. J., Abbott, M. R., Strub, P. T., Barber, R. T., Jessen, P., and Small, L. F.: The structure of the transition zone between coastal waters and the open ocean off northern California, winter and spring 1987, J. Geophys. Res., 96(8), 14707-14730, 1991.

Laruelle, G. G., Dürr, H. H., Slomp, C. P., and Borges, A. V.: Evaluation of sinks and sources of CO_2 in the global coastal ocean using a spatially-explicit typology of estuaries and continental shelves, Geophys. Res. Lett., 37, L15607, doi:10.1029/2010GL043691, 2010.

Lewis, E., and Wallace, D. W. R.: Program Developed for CO_2 System Calculations, ORNL/CDIAC-105, Carbon Dioxide Information Analysis Center, Oak Ridge National Laboratory, U.S. Department of Energy, Oak Ridge, TN, 1998.

Lohan, M. C., and Bruland, K. W.: The importance of vertical mixing for the supply of nitrate and iron to the Columbia River plume: Implications for biology, Mar. Chem., 98, 260-273, 2006.

Lynn, R. J., and Simpson, J. J.: The California Current system: The seasonal variability of its

physical characteristics, J. Geophys. Res., 92(12), 12947-12966, 1987.

Martz, T., Send, U., Ohman, M. D., Takeshita, Y., Bresnahan, P., Kim, H.-J., and Nam, S. H.: Dynamic variability of biogeochemical ratios in the Southern California Current System, Geophys. Res. Lett., 41, 2496-2501, doi:10.1002/2014GL059332, 2014.

Oke, P. R., Allen, J. S., Miller, R. N., Egbert, G. D., Austin, J. A., Barth, J. A., Boyd, T. J., Kosro, P. M., and Levine, M. D.: A modeling study of the three-dimensional continental shelf circulation off Oregon. Part I: Model-data comparisons, J. Phys. Oceanogr., 32, 1360-1382, 2002.

Park, K.: Columbia River plume identification by specific alkalinity, Limnol. Oceanogr., 11, 118-120, 1966.

Park, K.: Alkalinity and pH off the coast of Oregon, Deep-Sea Res., 15, 171-183, 1968.

Park, P. K., Catalfomo, M., Webster, G. R., and Reid, B. H.: Nutrients and carbon dioxide in the Columbia river, Limnol. Oceanogr., 15, 70-79, 1970.

Park, P. K., Gordon, L. I., Hager, S. W., and Cissell, M. C.: Carbon dioxide partial pressure in the Columbia river, Science, 166, 867-868, 1969a.

Park, P. K., Webster, G. R., and Yamamoto, R.: Alkalinity budget of the Columbia River, Limnol. Oceanogr., 14, 559-567, 1969b.

Redfield, A. C., Ketchum, B. H., and Richards, F. A.: The influence of organisms on the composition of seawater, in: The Sea, edited by M. N. Hill, Wiley, New York, 26-77, 1963.

Revelle, R., and Suess, H. E.: Carbon dioxide exchange between atmosphere and ocean and the question of an increase of atmospheric CO_2 during the past decades, Tellus, 9, 18-27, 1957.

Sambrotto, R. M., Savidge, G., Robinson, C., Boyd, P., Takahashi, T., Karl, D. M., Langdon, C., Chipman, D., Marra, J., and Codispoti, L.: Elevated consumption of carbon relative to

655 nitrogen in the surface ocean, Nature, 363, 248-250, 1993.
656 Santana-Casiano, J. M., González-Dávila, M., and Ucha, I. R.: Carbon dioxide fluxes in the
657 Benguela upwelling system during winter and spring: A comparison between 2005 and 2006,
658 Deep-Sea Res. II, 56, 533-541, 2009.
659 Sigleo, A. C., and Frick, W. E.: Seasonal variations in river flow and nutrient concentrations in a
660 northwestern USA watershed, in: First interagency conference on research in the watersheds,
661 edited by K. G. Renard, S. A. McElroy, W. J. Gburek, H. E. Canfield, and R. L. Scott, U.S.
662 Department of Agriculture, 370-376, 2003.
663 Snyder, M. A., Sloan, L. C., Diffenbaugh, N. S., and Bell, J. L.: Future climate change and
664 upwelling in the California Current, Geophys. Res. Lett., 30(15), 1823,
665 doi:10.1029/2003GL017647, 2003.
666 Spitz, Y. H., Allen, J. S., and Gan, J.: Modeling of ecosystem processes on the Oregon shelf
667 during the 2001 summer upwelling, J. Geophys. Res., 110, C10S17,
668 doi:10.1029/2005JC002870, 2005.
669 Sundquist, E. T., Plummer, L. N., and Wigley, T. M. L.: Carbon dioxide in the ocean surface: The
670 homogenous buffer factor, Science, 204, 1203-1205, 1979.
671 Sydeman, W. J., García-Reyes, M., Schoeman, D. S., Rykaczewski, R. R., Thompson, S. A.,
672 Black, B. A., and Bograd, S. J.: Climate change and wind intensification in coastal upwelling
673 ecosystems, Science, 345, 77-80, 2014.
674 Thomson, R. E., and Krassovski, M. V.: Poleward reach of the California Undercurrent
675 extension, J. Geophys. Res., 115, C09027, doi:10.1029/2010JC006280, 2010.
676 Torres, R., Turner, D. R., Rutllant, J., and Lefèvre, N.: Continued CO_2 outgassing in an
677 upwelling area off northern Chile during the development phase of El Niño 1997-1998 (July

678 1997), J. Geophys. Res., 108, 3336, doi:10.1029/2000JC000569, 2003.
679 Wetz, M. S., Hales, B., Chase, Z., Wheeler, P. A., and Whitney, M. M.: Riverine input of
680 macronutrients, iron, and organic matter to the coastal ocean off Oregon, U.S.A., during the
681 winter, Limnol. Oceanogr., 51, 2221-2231, 2006.
682 Wong, C. S., Waser, N. A. D., Nojiri, Y., Whitney, F. A., Page J. S., and Zeng, J.: Seasonal cycles
683 of nutrients and dissolved inorganic carbon at high and mid latitudes in the North Pacific
684 Ocean during the *Skaugran* cruises: determination of new production and nutrient uptake
685 ratios, Deep-Sea Res. II, 49, 5317-5338, 2002.

686 **Table 1.** $\Delta DIC - 6.6\Delta NO_3$, sea-air ΔpCO_2 and sea surface pCO_2 estimated with different DIC^{eff}, which is the combined freshwater end-

687 member of DIC partly sourced from the Columbia River (CR).

TAlk/DIC of CR ($\mu mol\ kg^{-1}$)	DIC^{eff} ($\mu mol\ kg^{-1}$)	$\Delta DIC - 6.6\Delta NO_3$ ($\mu mol\ kg^{-1}$)		Sea-air ΔpCO_2 (μatm)		Sea surface pCO_2 (μatm)	
		Transect 4		Transect 4		Transect 4	
		Stations 27-32[a]	Station 33[b]	Stations 27-32[a]	Station 33[b]	Stations 27-32[a]	Station 33[b]
800	435	−24±2	−24±1	−58±5	−55±3	332±5	335±3
1000	450	−23±2	−23±1	−55±5	−53±3	335±5	337±3
1200	460	−22±2	−22±1	−54±5	−53±3	336±5	337±3
		Transect 5 Stations 35-38[b]		Transect 5 Stations 35-38[b]		Transect 5 Stations 35-38[b]	
800	565	−21±3		−51±8		339±8	
1000	585	−20±3		−48±8		342±8	
1200	600	−20±3		−47±8		343±8	
		Transect 6 Stations 45-49[b]		Transect 6 Stations 45-49[b]		Transect 6 Stations 45-49[b]	
800	520	−24±3		−56±6		334±6	
1000	540	−23±3		−53±6		337±6	
1200	550	−23±3		−53±6		337±6	

688 [a] data for these stations were obtained from waters immediately below the top buoyant layer.

689 [b] data for these stations were obtained from the surface mixed layer.

690 **Table 2.** $\Delta DIC - 6.6\Delta NO_3$, sea-air ΔpCO_2 and sea surface pCO_2 estimated with the deep water end-member from different depths.

Depth of the deep water end-member (m)	$\Delta DIC - 6.6\Delta NO_3$ ($\mu mol\ kg^{-1}$)		Sea-air ΔpCO_2 (μatm)		Sea surface pCO_2 (μatm)	
	Transect 4		Transect 4		Transect 4	
	Stations 27-32[a]	Station 33[b]	Stations 27-32[a]	Station 33[b]	Stations 27-32[a]	Station 33[b]
~130	−23±2	−19±1	−56±5	−45±3	334±5	345±3
~150	−23±2	−22±1	−55±5	−52±3	335±5	338±3
~175	−23±2	−23±1	−55±5	−53±3	335±5	337±3
~200	−23±2	−24±1	−55±5	−56±3	335±5	334±3
	Transect 5		Transect 5		Transect 5	
	Stations 35-38[b]		Stations 35-38[b]		Stations 35-38[b]	
~130	−21±3		−51±8		339±8	
~150	−20±3		−46±8		344±8	
~175	−20±3		−48±8		342±8	
~200	−17±3		−40±8		350±8	
	Transect 6		Transect 6		Transect 6	
	Stations 45-49[b]		Stations 45-49[b]		Stations 45-49[b]	
~130	−20±3		−46±6		344±6	
~150	−22±3		−51±6		339±6	
~175	−23±3		−53±6		337±6	
~200	−21±3		−50±6		340±6	

691 [a] data for these stations were obtained from waters immediately below the top buoyant layer.

692 [b] data for these stations were obtained from the surface mixed layer.

693 **Table 3.** Sea-air ΔpCO_2 and sea surface pCO_2 estimated with different $\Delta DIC - x\Delta NO_3$. x denotes the C/N uptake ratio during organic carbon

694 production. T and S represent transect and station(s).

C/N uptake ratio	$\Delta DIC - x\Delta NO_3$ ($\mu mol\ kg^{-1}$)				Sea-air ΔpCO_2 (μatm)				Sea surface pCO_2 (μatm)			
	T4		T5	T6	T4		T5	T6	T4		T5	T6
	S27-32[a]	S33[b]	S35-38[b]	S45-49[b]	S27-32[a]	S33[b]	S35-38[b]	S45-49[b]	S27-32[a]	S33[b]	S35-38[b]	S45-49[b]
6.6[c]	−23±2	−23±1	−20±3	−23±3	−55±5	−53±3	−48±8	−53±6	335±5	337±3	342±8	337±6
7.3[d]	−42±3	−42±1	−39±3	−42±3	−101±6	−100±3	−92±8	−97±6	289±6	290±3	298±8	293±6

695 [a] data for these stations were obtained from waters immediately below the top buoyant layer.

696 [b] data for these stations were obtained from the surface mixed layer.

697 [c] 6.6 is the Redfield C/N uptake ratio (approximately 106/16; Redfield et al., 1963).

698 [d] 7.3 is the more recent evaluation of the C/N uptake ratio (approximately 117/16; Anderson and Sarmiento, 1994).

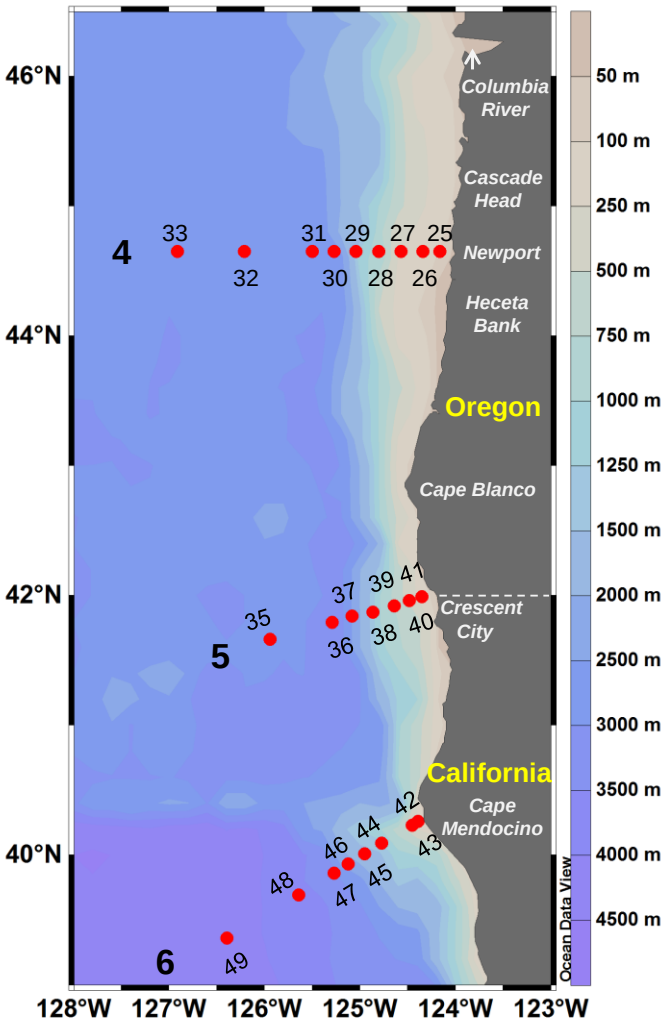

699

700 **Fig. 1.** Map of the US west coast off Oregon and northern California showing the topography

701 and the locations of sampling stations along Transects 4, 5 and 6 in spring/early summer 2007.

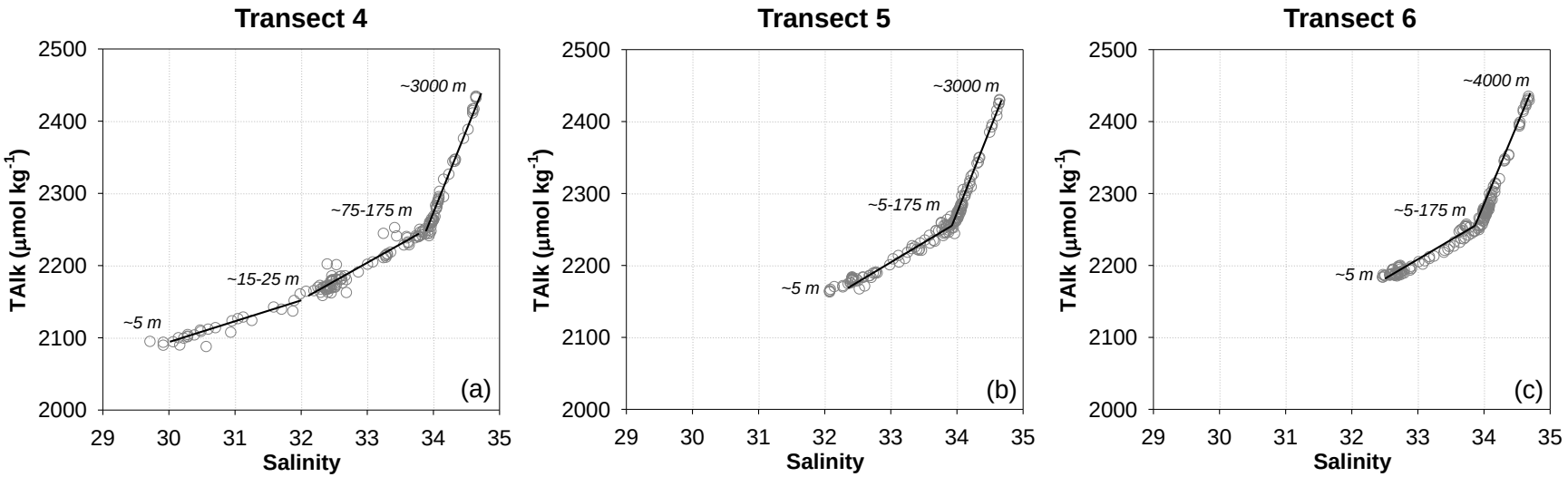

Fig. 2. Total alkalinity versus salinity through the entire water column of sampling stations along Transects 4 (a), 5 (b) and 6 (c) off Oregon and northern California in spring/early summer 2007. The solid lines indicate various linear relationships observed on each transect. The numbers in italics denote the sampling depth/depth range of the endpoints of each line.

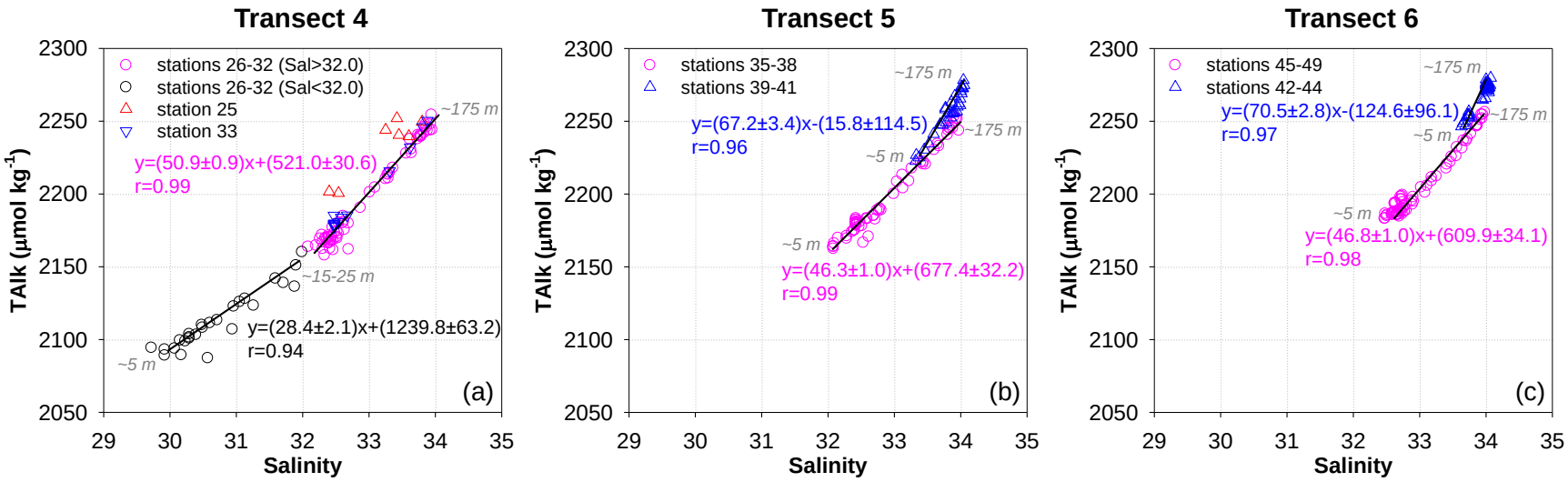

706

707 **Fig. 3.** Total alkalinity versus salinity (TAlk-Sal relationship) in the upper 175 m waters of sampling stations along Transects 4 (a), 5
708 (b) and 6 (c) off Oregon and northern California in spring/early summer 2007. The solid lines as well as the equations (in accordance
709 with the symbol colors) indicate the linear regression analyses of the TAlk-Sal relationship for various stations. The numbers in italics
710 denote the sampling depth/depth range of the endpoints of each line. In (a), the TAlk-Sal relationship at station 26-32 displayed two
711 phases for waters with salinity lower and higher than ~32.0. The top waters at these stations were imprinted by the Columbia River
712 plume. The data points of bottom waters at stations 26 (~75 m) and 27 (~130 m and ~160 m) were not included, as they were located
713 on the third linear relationship shown in Fig. 2a. In (b) and (c), stations 39-41 and stations 42-44 were largely influenced by coastal
714 upwelling.

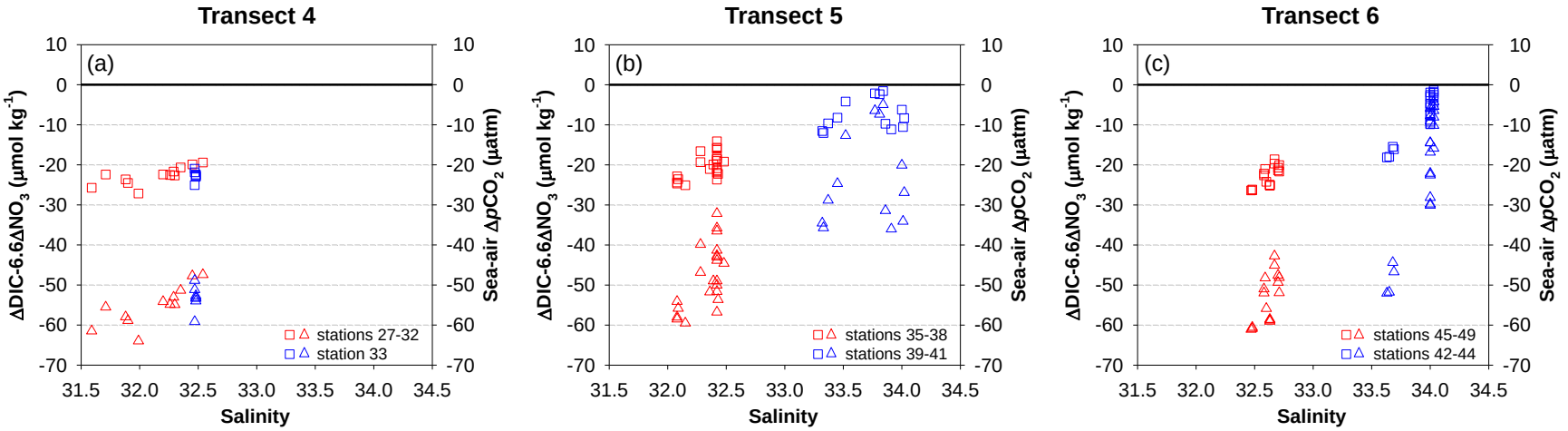

715

716 **Fig. 4.** $\Delta DIC - 6.6\Delta NO_3$ (squares) and sea-air ΔpCO_2 (triangles) versus salinity in the upper waters on Transects 4 (a), 5 (b) and 6 (c)
717 off Oregon and northern California in spring/early summer 2007. Note that data for stations 27-32 on Transect 4 were obtained from
718 waters immediately below the top buoyant layer, while data for other stations were obtained from the surface mixed layer. The value
719 of 6.6 is the Redfield C/N uptake ratio (approximately 106/16; Redfield et al., 1963). The solid line indicates the pCO_2 equilibrium
720 between the seawater and the atmosphere.

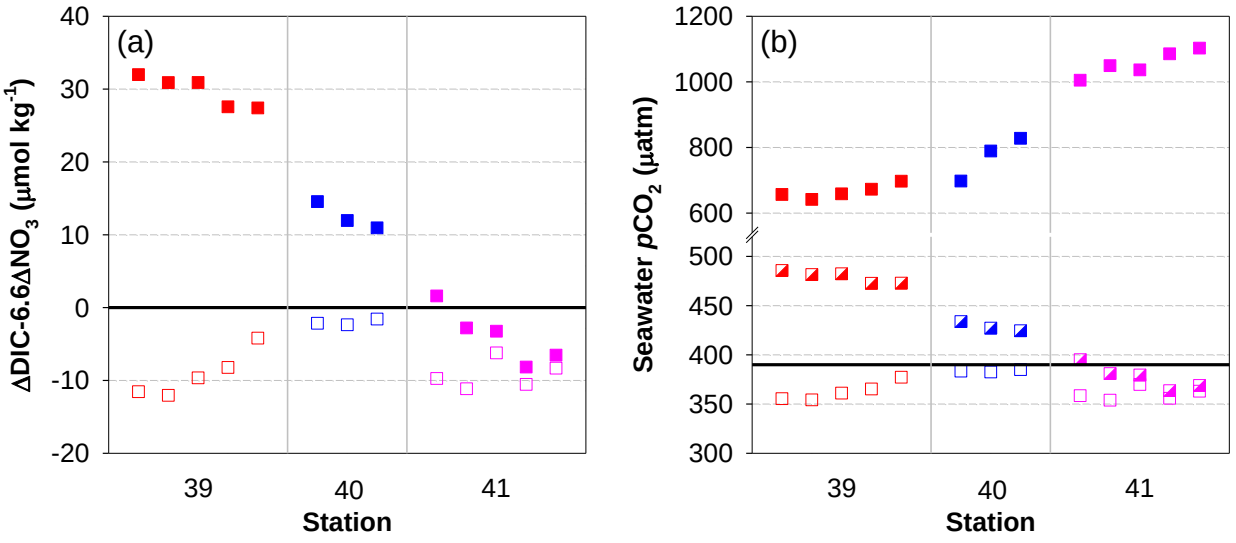

721

722 **Fig. 5.** ΔDIC−6.6ΔNO$_3$ (a) and seawater pCO_2 (b) in the surface mixed layer at stations 39-41 on
723 Transect 5 near the Oregon-California border in spring/early summer 2007. In (a), open symbols
724 indicate values estimated based on the two end-member mixing between the upwelling source
725 water and the rainwater, while filled symbols indicate values after removing the rainwater. The
726 value of 6.6 is the Redfield C/N uptake ratio (approximately 106/16; Redfield et al., 1963). The
727 solid line indicates the pCO_2 equilibrium between the seawater and the atmosphere. In (b), the
728 open and semi-filled symbols denote the estimated sea surface pCO_2 from ΔDIC−6.6ΔNO$_3$ on
729 top of the mixing with and without rainwater, respectively. The filled symbols denote the field
730 observed sea surface pCO_2, which were obtained by applying TAlk and DIC data into the
731 CO2SYS program (Lewis and Wallace, 1998). The solid line denotes the atmospheric pCO_2 of
732 ~390 μatm (Evans et al., 2011).

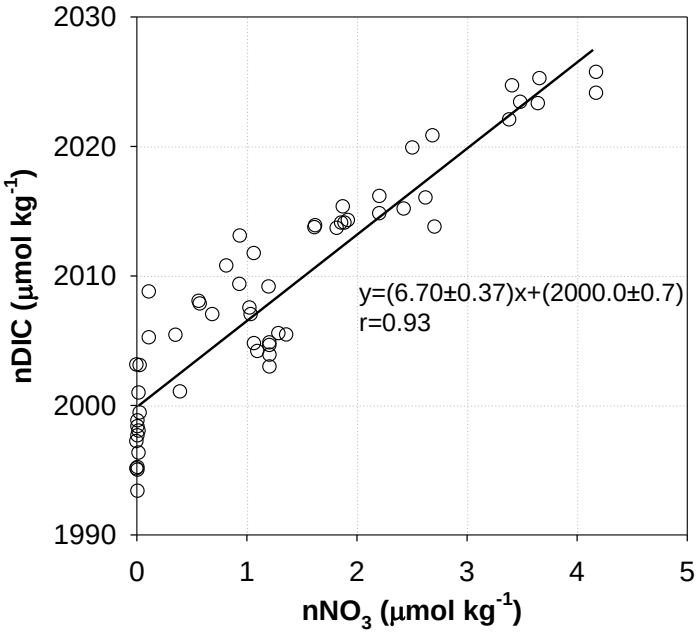

733

734 **Fig. 6.** Salinity normalized DIC (nDIC) versus salinity normalized NO_3 (nNO_3) in the CO_2 sink
735 zones off Oregon and northern California in spring/early summer 2007, which included waters
736 immediately below the top buoyant layer at stations 27-32 as well as waters in the surface mixed
737 layer at station 33 on Transect 4, waters in the surface mixed layer at stations 35-38 on Transect
738 5, and waters in the surface mixed layer at stations 45-49 on Transect 6.